Molecular Biology of the Cell
Vol. 20, 2820–2830, June 15, 2009

The Mating-specific Gα Interacts with a Kinesin-14 and Regulates Pheromone-induced Nuclear Migration in Budding Yeast

Sofia V. Zaichick,*†‡ Metodi V. Metodiev,*†§ Scott A. Nelson,†‖ Oleksii Durbrovskyi,* Edward Draper,*¶ John A. Cooper,‖ and David E. Stone*

*Laboratory for Molecular Biology, Department of Biological Sciences, University of Illinois at Chicago, Chicago, IL 60607; and ‖Department of Cell Biology and Physiology, Washington University in St. Louis, St. Louis, MO 63110

Submitted January 23, 2009; Revised April 8, 2009; Accepted April 14, 2009
Monitoring Editor: Daniel J. Lew

As a budding yeast cell elongates toward its mating partner, cytoplasmic microtubules connect the nucleus to the cell cortex at the growth tip. The Kar3 kinesin-like motor protein is then thought to stimulate plus-end depolymerization of these microtubules, thus drawing the nucleus closer to the site where cell fusion and karyogamy will occur. Here, we show that pheromone stimulates a microtubule-independent interaction between Kar3 and the mating-specific Gα protein Gpa1 and that Gpa1 affects both microtubule orientation and cortical contact. The membrane localization of Gpa1 was found to polarize early in the mating response, at about the same time that the microtubules begin to attach to the incipient growth site. In the absence of Gpa1, microtubules lose contact with the cortex upon shrinking and Kar3 is improperly localized, suggesting that Gpa1 is a cortical anchor for Kar3. We infer that Gpa1 serves as a positional determinant for Kar3-bound microtubule plus ends during mating.

INTRODUCTION

The regulation of the actin and microtubule cytoskeletons by external stimuli is essential to many fundamental processes in eukaryotic cells, including chemotaxis, differentiation, morphogenesis, and secretion (Acuto and Cantrell, 2000; Musch, 2004; Affolter and Weijer, 2005; Bardwell, 2005). The mating reaction of the budding yeast, *Saccharomyces cerevisiae*, is an excellent model with which to study signal-induced changes in cytoskeletal polarity and organelle position. During the haploid phase of their life cycle, yeast cells secrete peptide pheromones that transform vegetatively growing cells of opposite mating type into gametes. Preparatory to cellular and nuclear fusion, pheromone triggers the induction of mating-specific genes, cell cycle arrest, polarized growth toward the mating partner, and nuclear migration to the tip of the mating projection (Rose, 1996; Madden and Snyder, 1998; Bardwell, 2005).

The molecular mechanisms underlying transmission of the mating signal to the nucleus are well understood. Communication of the signal across the plasma membrane is mediated by a G protein-coupled receptor (Bardwell, 2005). When occupied by ligand, the pheromone receptors activate the pheromone-responsive Gα protein (Gpa1) via guanine nucleotide exchange and the subsequent dissociation of Gα-GTP from the Gβγ dimer. The signal is then transmitted by Gβγ through a Pak kinase and a scaffolding protein to a mitogen-activated protein (MAP) kinase cascade. Upon activation in the cytoplasm, the Fus3 MAP kinase accumulates in the nucleus (Choi *et al*., 1999; vanDrogen *et al*., 2001; Blackwell *et al*., 2003), where it induces mating-specific transcription and cell cycle arrest.

In addition to regulating transcription and cell proliferation, pheromone elicits directional responses: directed growth of the mating projection and movement of the nucleus into it (Rose, 1996; Madden and Snyder, 1998). In a mating mixture, a yeast cell determines the direction of the strongest source of pheromone and orients its axis of polarity toward the closest potential mating partner (Jackson and Hartwell, 1990). The first known step in this process is the spatial rearrangement of the pheromone receptor. In response to pheromone stimulation, the distribution of the receptor on the cell surface changes from uniform to a polarized crescent (Ayscough and Drubin, 1998). The βγ subunit of the associated G protein is an early positional determinant of the growth site (Butty *et al*., 1998; Nern and Arkowitz, 1999). Gβγ recruits Far1 from the nucleus and the Gβγ–Far1 complex competes with the bud site determinant Bud1 to specify where actin cables will be nucleated via Cdc42 and its effectors (Nern and Arkowitz, 1999). The pheromone-responsive Gα protein also influences actin polarity (Matheos *et al*., 2004), at least in part by recruiting active Fus3 to phosphorylate the formin Bni1, a member of the polarisome complex. Once the actin cables are polymerized and correctly oriented, a myosin motor protein, Myo2, moves vesicles containing plasma membrane and cell wall constituents, as well as many of the signaling molecules, to the growth site (Pruyne *et al*., 2004).

Nuclear migration depends on the dynamic instability of cytoplasmic microtubules that grow from the spindle pole

This article was published online ahead of print in *MBC in Press* (http://www.molbiolcell.org/cgi/doi/10.1091/mbc.E09–01–0069) on April 22, 2009.

† These authors contributed equally to this work.

Present addresses: ‡ Department of Microbiology and Immunology, Northwestern University, 303 East Chicago Ave., Chicago, IL 60611; § Department of Biological Sciences, University of Essex, Wivenhoe Park, Colchester, Essex CO4 3SQ, United Kingdom; ¶ Department of Pharmacology, Loyola University Medical School, Maywood, IL 60153.

Address correspondence to: David E. Stone (dstone@uic.edu).

Table 1. Yeast strains used in this study

Strain	Background	Genotype	Source
SLY111	BF264-15D	*MAT***a** *bar1*Δ *ade1 his2 leu2-3,112 trp1-1a ura3*Δ *gpa1*Δ*::URA3* YCplac111/GPA1-GFP	This study
SZY123	BF264-15D	*MAT***a** *bar1*Δ *ade1 his2 leu2-3,112 trp1-1a ura3*Δ pRS316CG/KAR3-GFP	This study
SZY125	BF264-15D	*MAT***a** *bar1*Δ *ade1 his2 leu2-3,112 trp1-1a ura3*Δ YCplac22/KAR3-GFP	This study
SZY126	BF264-15D	*MAT***a** *bar1*Δ *ade1 his2 leu2-3,112 trp1-1a ura3*Δ *gpa1*Δ*::URA3* YIplac128/GAL1^{EG43}-GPA1 YCplac22/KAR3-GFP	This study
SLY168	BF264-15D	*MAT***a** *bar1*Δ *ade1 his2 leu2-3,112 trp1-1a ura3*Δ *gpa1*Δ*::URA3* YIplac128/GAL1^{EG43}-GPA1	Stone laboratory
SLY245	BF264-15D	*MAT***a** *bar1*Δ *ade1 his2 leu2-3,112 trp1-1a ura3*Δ pRS316CG/GPA1-GFP	This study
SZY254	BF264-15D	*MAT***a** *bar1*Δ *ade1 his2 leu2-3,112 trp1-1a, ura3*Δ pbj1351/GFP-TUB1	This study
SZY257	BF264-15D	*MAT***a** *bar1*Δ *ade1 his2 leu2-3,112 trp1-1a, ura3*Δ pRS316CG/GPA1-GFP	Stone laboratory
SZY267	BF264-15D	*MAT***a** *bar1*Δ *ade1 his2 leu2-3,112 trp1-1a, ura3*Δ YCplac22/GAL1-GPA1-GFP	Stone laboratory
SZY270	BF264-15D	*MAT***a** *bar1*Δ *ade1 his2 leu2-3,112 trp1-1a, ura3*Δ DSB132/GAL1-GPA1 YCplac22/KAR3-GFP	This study
SZY274	BF264-15D	*MAT***a** *bar1*Δ *ade1 his2 leu2-3,112 trp1-1a, ura3*Δ *gpa1*Δ*::URA3* YCPlac22/GPA1	Stone laboratory
SSY370	BF264-15D	*MAT***a** *bar1*Δ *ade1 his2 leu2-3,112 trp1-1a ura3*Δ *kar3*Δ*::kan*	This study
SZY136	TBY101	*MAT***a** *bar1*Δ *ade1 his2 leu2-3,112 trp1-1a ura3*Δ *gpa1^{ts}*	Stone laboratory
SZY138	BF264-15D	*MAT***a** *bar1*Δ *ade1 his2 leu2-3,112 trp1-1a, ura3*Δ *gpa1*Δ*::URA3* YCPlac22/GPA1	Stone laboratory
SZY143	TBY101	*MAT***a** *bar1*Δ *ade1 his2 leu2-3,112 trp1-1a ura3*Δ *gpa1^{ts} pRS316CG/KAR3-GFP*	Stone laboratory
SZY145	TBY101	*MAT***a** *bar1*Δ *ade1 his2 leu2-3,112 trp1-1a ura3*Δ *gpa1^{ts} YCplac22/KAR3-GFP*	Stone laboratory
SZY147	BY4741	*MAT***a** *his3*Δ*1 leu2*Δ*0 met15*Δ*0 ura3*Δ*0*	Δ library
SZY148	BY4741	*MAT***a** *his3*Δ*1 leu2*Δ*0 met15*Δ*0 ura3*Δ*0 kar3::kan*	Δ library
SZY165	BY4741	*MAT***a** *his3*Δ*1 leu2*Δ*0 met15*Δ*0 ura3*Δ*0* pRS316CG/KAR3-GFP	This study
SZY166	BY4741	*MAT***a** *his3*Δ*1 leu2*Δ*0 met15*Δ*0 ura3*Δ*0 kar3::kan* pRS316CG/KAR3-GFP	This study
SZY169	BY4741	*MAT***a** *his3*Δ*1 leu2*Δ*0 met15*Δ*0 ura3*Δ*0 cik1::kan*	Δ library
SZY172	BY4741	*MAT***a** *his3*Δ*1 leu2*Δ*0 met15*Δ*0 ura3*Δ*0 cik1::kan* pRS316CG/KAR3-GFP	This study
SZY190	BY4741	*MAT***a** *his3*Δ*1 leu2*Δ*0 met15*Δ*0 ura3*Δ*0 GAL1-HO-URA3*	This study
SZY230	BY4741	*MAT***a** *his3*Δ*1 leu2*Δ*0 met15*Δ*0 ura3*Δ*0 vik1::kan*	This study
Y1870		*MAT***a** *bar1*Δ *ade1 his2 leu2-3,112 trp1-1a, ura3*Δ Kar3-HAT::URA3	Manning *et al.* (1999)

body (SPB) and which attach the nucleus to the cortex at the tip of the mating projection, or shmoo (Rose, 1996; Maddox *et al*., 1999). A Myo2-Kar9-Bim1 complex transports the plus ends of these microtubules into the mating projection along the polarized actin cables (Hwang *et al*., 2003). In mating projections, there is typically a bundle of three to four cytoplasmic microtubules attached to the shmoo tip, as well as one to two free microtubules (Maddox *et al*., 1999). Both the free and attached microtubules grow and shrink periodically (Maddox *et al*., 1999, 2003). It has been proposed that polymerizing microtubules are connected to the cortex by Bim1 and Kar9 (Maddox *et al*., 2003). As these microtubules lengthen, the nucleus is pushed away from the shmoo tip. The nucleus is drawn toward the shmoo tip, in contrast, when the attached microtubules shorten (Maddox *et al*., 1999, 2003). This requires Kar3, a minus-end–directed kinesin-like motor protein, and one of its light chains, Cik1 (Maddox *et al*., 2003; Sproul *et al*., 2005). In response to pheromone stimulation, Kar3 and Cik1 localize to the plus ends of cytoplasmic microtubules in an interdependent manner (Page *et al*., 1994; Maddox *et al*., 2003). At the shmoo tip, Kar3-Cik1 is thought to promote the persistent depolymerization of the associated microtubules (Maddox *et al*., 2003; Sproul *et al*., 2005) and to maintain their cortical interaction as they shorten (Maddox *et al*., 2003). Thus, the nucleus is pulled to the site where cell fusion and karyogamy will occur. It is not known, however, how Kar3 is anchored to the shmoo tip, nor how pheromone regulates Kar3 function at the cortex.

Here, we show that the pheromone-responsive Gα protein, Gpa1, interacts with Kar3 and that it positions the plus ends of cytoplasmic microtubules at the cortex of the shmoo tip. Like Kar3, Gpa1 seems to promote the shrinkage of these microtubules while helping to maintain their cortical contact. Thus, Gpa1 may serve both to anchor Kar3 at the cortex and to stimulate its activity. Our data reveal a novel mechanism for communicating external signals to the microtubule cytoskeleton. Interestingly, $G\alpha_{12/13}$ proteins in mouse embryonic fibroblasts have also been recently implicated in linking extracellular signals to microtubule dynamics and cell polarity, albeit via a distinct mechanism (Goulimari *et al*., 2008).

MATERIALS AND METHODS

Yeast Strains and Culture Conditions

The yeast strains used in this study are listed in Table 1. All are derivatives of either strain BF264-15D (*MAT***a** *bar1*Δ *ade1 his2 leu2-3112 trp1-1a ura3*Δ) (Reed *et al*., 1985) or strain BY4741 (*MAT***a** *GF554 his3*Δ*1 leu2*Δ*0 met15*Δ*0 ura3*Δ*0 BAR1*) (Winzeler *et al*., 1999), with the exception of the *gpa1^{ts}* strain and strain Y1870 in which Kar3 was hemagglutinin (HA)-tagged in situ (Manning *et al*., 1999). The *gpa1^{ts}* allele was originally isolated in strain 381G, but it was backcrossed three times to BF264-15D to generate the strain used in this work. The Gpa1 overexpression/turn-off strain SLY168 was constructed by replacing the coding region of *GPA1* with that of *URA3* and integrating the *GAL1^{EG43}-GPA1* transcriptional fusion at the *LEU2* locus by using YIplac128 (Gietz and Sugino, 1988). The GPA1-green fluorescent protein (GFP) and GAL1-GPA1-GFP reporter strains were generated by transforming SLB126 and SLB127 (see below) into DSY296, a *MAT***a***/MATa gpa1*Δ*::URA3/gpa1*Δ*::URA3* strain derived from BF264-15D, sporulating the transformants, and isolating *MAT***a** GPA1-GFP (SLY111) and *MAT***a** GAL1-GPA1-GFP (SZY267) segregants. The complete deletion of *KAR3* in SLY168 was generated by homologous recombination using the KanMX6 cassette polymerase chain reaction (PCR)-amplified with flanking *KAR3* sequence (Wach, 1996) to yield strain SLY370. All yeast manipulations were performed as described previously (Sherman *et al*., 1986).

Plasmid Construction

The plasmids used in this study are listed in Table 2. The key details of the newly constructed plasmids are described below. Recombinant DNA techniques were essentially as described by Ausubel *et al*. (1994). The *GPA1* locus (−817 to 1420) was PCR amplified from a genomic template using the following primers: 5′-ACGCGTCGACAGAATGAATCTTCGTGCCTAG-3′, which contains a SalI site, and 5′-CGTAGCGGCCGCATATAATACCAATTTTTTTAAGGTTTTG-3′, which contains a NotI site. The Gpa1 PCR product was then subcloned into SalI-NotI-cut pRS316CG (Liu and Lindquist, 1999) to create the in-frame GPA1-GFP translational fusion pRS316CG/GPA1-GFP (SZB100). To change selectable markers, the SacI-SalI fragment containing GPA1-GFP in

Table 2. Plasmids used in this study

Plasmid no.	Plasmid name	Marker/plasmid type	Source
SZB100	pRS316CG/GPA1-GFP	URA3/CEN	This study
SZB146	pRS316CG/KAR3-GFP	URA3/CEN	This study
SZB148	YCplac22/KAR3-GFP	TRP1/CEN	This study
SZB151	pRS316CG/CUP-GFP	URA3/CEN	Susan Lindquist (Whitehead Institute for Biomedical Research, Cambridge, MA)
SZB177	pbj1333/GFP-TUB1	URA3/INT	John Cooper (Washington University, St. Louis, MO)
SZB178	pbj1351/GFP-TUB1	LEU2/INT	John Cooper
SLB126	YCplac111/GPA1-GFP	LEU2/CEN	This study
SLB253	YCplac22/GAL1-GPA1-GFP	TRP1/CEN	Stone laboratory
DSB132	YCpG2/GAL1-GPA1	URA3-LEU2/2μ	Stone laboratory
MMB100	pYEX-4T/GST-GPA1	URA3/2μ	Metodiev *et al.* (2002)
EJ758	pYEXdelta/Cup-Kar3-GST	URA3/CEN	Martzen *et al.* (1999)

SZB100 was moved to YCplac111 (Gietz and Sugino, 1988), yielding YCplac111/GPA1-GFP (SLB126). The GAL1-GPA1-GFP reporter was created by PCR amplifying the GPA1-GFP fusion contained on YCplac111/GPA1-GFP (SLB126) using the following primers: 5′ GACTTTCTAGAATGGGGTGTACAGTGAGTACGC-3′, which contains a XbaI site, and 5′-GACTTCTGCAGTCATTTGTATAGTTCATCCATGCC-3′, which contains a PstI site. The PCR product was then subcloned into XbaI-PstI-cut pZWB159 (Blackwell *et al*., 2003) to generate SLB253. The *KAR3* locus (1-2247) was PCR amplified from a genomic template by using the following primers: 5′-GGCGCGGATCCATGGAATCACTTCCACGTACTCC-3′, which contains a BamHI site, and 5′-GCGCGAGCTCGGACAGTCTCTGTCATTTGTCAAA-3′, which contains a SacI site. The *KAR3* PCR product was then subcloned into BamHI-SacI-cut pGEX-KG (Stratagene, La Jolla, CA) to create the in-frame *GAL1-GST-KAR3* translational fusion pGEX-KG/GST-KAR3 (SZB104). The *KAR3* locus (−423 to 2190) was PCR amplified from a genomic template by using the following primers: 5′-CGCGCGGTCGACTTATTGTATCTTTTTCCGGCTCAT-3′, which contains a SalI site, and 5′-GCGCGGATCCCCGCATTTTCTACTAACCAATCTGGTAGAAT-3′, which contains a BamHI site, a modified stop codon, and two extra base pairs. The *KAR3* PCR product was then subcloned into SalI-BamHI-cut pRS316CG to create the in-frame *KAR3-GFP* translational fusion pRS316CG/KAR3-GFP (SZB146). To move the Kar3-GFP fusion to a *TRP1* centromeric plasmid, the SZB146 SalI-SacI fragment containing *KAR3-GFP* was subcloned into SalI-SacI-cut YCplac22 (Gietz and Sugino, 1988), thereby creating YCplac22/KAR3-GFP (SZB147).

Affinity Purifications and Mass Spectrometry

The affinity-copurification, high-resolution two-dimensional electrophoresis and mass spectrometry procedures used in identifying the Gpa1-Kar3 interaction in vivo have been described previously (Metodiev *et al*., 2002). The native forms of Gpa1 were identified on immunoblots using an anti-Gpa1 polyclonal antibody (Stone *et al*., 1991). The mass spectrometric data matching to Kar3 are shown in the Supplemental Figure 1.

Nuclear Migration and Karyogamy Assays

To assay pheromone-induced nuclear migration, mid-log phase cells were treated with 18–30 nM synthetic α-factor (MPS, San Diego, CA) for 3 h and stained with 4′-6-diamidino-2-phenylindole (DAPI) (Sigma-Aldrich, St. Louis, MO) as follows: 1-ml aliquots were collected, fixed with 70% ethanol for 20 min at room temperature, and DAPI was added to a final concentration of 0.1–0.2 μg/ml. After 12 min, cells were washed twice and resuspended in 20–50 μl of 1× phosphate-buffered saline (PBS). Fluorescent and differential interference contrast (DIC) images were then acquired using an Axioskop 2 microscope (Carl Zeiss, Thornwood, NY) fitted with a 63× oil immersion objective (total magnification, 630×) and an AxioCam digital camera (Carl Zeiss), and processed with AxioVision software (Carl Zeiss). Images were analyzed using Adobe Photoshop (Adobe Systems, Mountain View, CA) and ImageJ (National Institutes of Health, Bethesda, MD). Nuclear position (the coefficient of proximity) was calculated as the ratio of the shmoo tip to nucleus distance and the cell length. To assay karyogamy, 10^6 mid-log phase *gpa1^{ts}* cells of each mating type were mixed and aspirated onto 0.45 μm MFTM-Membrane filters (Millipore, Billerica, MA). The filters were then incubated at 25 or 37°C on rich medium for 2, 3, and 4 h. The resulting mating mixtures were washed off the filters, sonicated briefly, and stained with DAPI. Fluorescent and DIC images were taken, superimposed using Adobe Photoshop (Adobe Systems), and scored for the percentage of binucleate zygotes.

Gpa1 localization

*gpa1*Δ cells transformed with the GPA1-GFP plasmid were grown to mid-log phase in glucose medium and treated with 20 nM α-factor. Wild type cells transformed with the GAL1-GPA1-GFP plasmid were grown to mid-log phase in sucrose medium, and galactose was added to 3% 1 h before treatment with 38 nM α-factor. The cultures were sampled at 0, 30, 60, and 150 min after pheromone treatment, and fluorescent images were acquired as described above. ImageJ was used to analyze the data. The outline of each cell was traced using the "segmented line" feature and the intensity of fluorescent signal around the cell periphery was quantified using the "plot profile" function. For a small number of cells, the "find edges" function was used to aid in tracing, but this function was turned off before signal quantification. The data for each cell was pasted into an Excel file (Microsoft, Redmond, WA) programmed to calculate the polarity indices. For cells that had not yet formed a mating projection, the mean intensity in the brightest fourth of the plasma membrane was divided by the mean signal intensity in the opposite quarter of the plasma membrane. For shmooing cells, the mean intensity in brightest seventh of the membrane was divided by the mean intensity in the opposite seventh of the plasma membrane. Only randomly selected unbudded cells were scored. Cells expressing the wild type Gpa1-GFP reporter were assayed in selective glucose medium.

Microtubule Dynamics and Cortical Interactions

For time-lapse movie analysis of the wild type strain expressing *GFP-TUB1*, cells were grown overnight in rich glucose medium to mid-log phase and treated with 30 nM α-factor (Sigma-Aldrich) 60–90 min before movie acquisition. In the Gpa1 deficiency and overexpression experiments, *GAL1^{EG43}-GPA1* (SLY168) cells expressing *GFP-TUB1* were grown overnight in rich media containing 2% galactose and switched to glucose (Gpa1 turn-off) or fresh galactose (Gpa1 excess) 2 h before addition of α-factor. In the Gpa1 inactivation experiments, *gpa1^{ts} GFP-TUB1* cells were grown overnight in rich glucose medium at 25°C, treated with 30 nM α-factor for 1 h, and then shifted to 37°C and cultured for an additional hour before data acquisition. Ten-minute movies were collected at the rate of one frame per 2 s on a BX52 fluorescence microscope (Olympus, Melville, NY) equipped with a CSU-10 spinning disk confocal box (Yokogawa, Newnan, GA), a 160-mW 450- to 515-nm argon laser (National Laser, Salt Lake City, UT), and a XR Mega10 photointensified camera by Stanford Photonics (Palo Alto, CA). A 100× oil immersion objective was used (total magnification, 1500×). All time-lapse images were collected using In Vivo imaging software (QED Imaging, Pittsburgh, PA) and analyzed using ImageJ. Still images of cells expressing *GFP-TUB1* and *KAR3-GFP* were taken and processed with the Axioskop 2 setup described above. Student's *t* test was used to determine statistically significant differences in microtubule dynamics and Kar3-GFP localization.

Kar3-GFP Localization and Fluorescence Recovery after Photobleaching (FRAP) Analysis

Strains expressing *KAR3-GFP* were cultured as described for the time-lapse movie analysis (above), except that the *gpa1^{ts}* cells were shifted to restrictive temperature concomitant with pheromone treatment. For FRAP analysis, cells were placed in a growth chamber for time-lapse multimode imaging as described previously (Maddox *et al*., 2000). All imaging was performed at 25°C on an Eclipse TE2000-U inverted microscope (Nikon, Tokyo, Japan) equipped with a 1.4 numerical aperture 100× DIC objective. Single focal plane images were captured by an Orca ER digital camera (Hamamatsu Photonics, Hamamatsu City, Japan) by using a 400-ms epifluorescence exposure time (binned 2 × 2, central 600 × 600 pixel image frame, 1 pixel = 133 nm) and a 200-ms DIC exposure time. Cells were photobleached using the 488-nm line from a 100-mW argon laser (Spectra Physics, San Jose, CA) controlled by a sliding filter cube set (Conix Research, Springfield, OR). Cells were photobleached with two 35-ms laser pulses to ~5–15% of the prebleached fluorescence intensity. During image acquisition, one prebleach data point was recorded, followed by at least 20–25 data points every 2 s. The total imaging

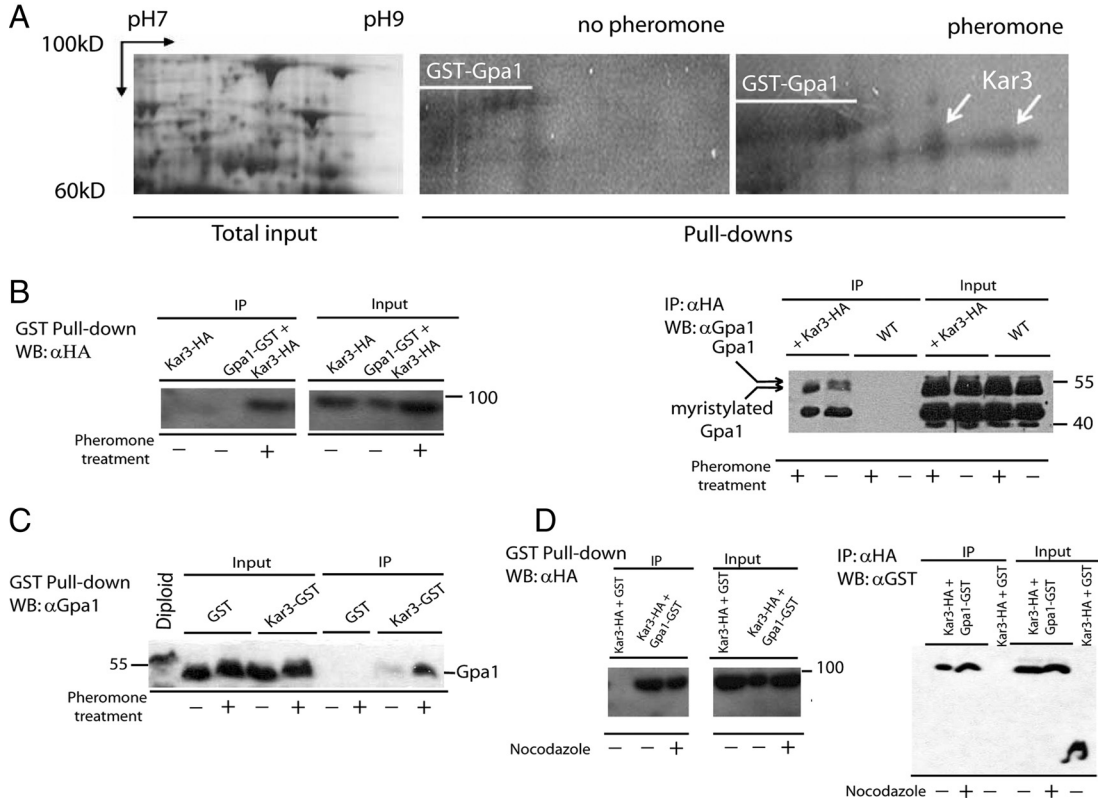

Figure 1. Identification and characterization of the Gpa1-Kar3 interaction. (A) Identification of Kar3 as a Gpa1 interactor in pheromone-treated cells. Proteins that copurify with GST-Gpa1 were run on Immobulin two-dimensional gels. The thin white line indicates the positions of GST-Gpa1, which runs as multiple spots, and the white arrows indicate the two spots identified as Kar3 by peptide mass fingerprinting. The gel fragments encompass the region from molecular weight 60–100 kDa and p*I* of 7–9. Left, input. Middle, GST-Gpa1 pull-down from untreated cells. Right, GST-Gpa1 pull-down from pheromone-treated cells. (B) Reciprocal copurification of Gpa1 and Kar3 from yeast lysates. Left, pull-down of Kar3-HA with GST-Gpa1. Right, immunoprecipitation of Gpa1 with Kar3-HA. (C) Pheromone-stimulation of the Gpa1–Kar3 interaction does not depend on the induction of *KAR3* transcription. Pull-down of Kar3-GST expressed from the *CUP1* promoter. (D) The Gpa1–Kar3 interaction does not depend on polymerized microtubules. Left, pull-down of Kar3-HA with GST-Gpa1. Right, immunoprecipitation of Gpa1 with Kar3-HA.

time was at least 40 s. Recovery was not significantly altered by photobleaching for up to 30 3-s frames, in comparison with images acquired from unbleached cells (Maddox *et al*., 2000).

Measurements of FRAP were made on a maximum-brightness projection of *z*-series for each time point from time-lapse sequences at 2-s intervals. A 5 pixel × 5 pixel square (corresponding to an area of 0.66 × 0.66 mm) was placed over the bleached plus end of the microtubule, spindle pole body, or a cytoplasmic reference site (for subtracting background), and the integrated intensity was measured three independent times for each set of data. The mean intensity was determined as follows: After exporting from MetaMorph (Molecular Devices, Sunnyvale, CA) to Excel 2000 (Microsoft), the data were corrected for background intensity and the photobleaching that takes place during image acquisition (correction derived from an average value of seven to 10 unirradiated cells observed under the experimental conditions at corresponding stages of the pheromone response or cell cycle) and then normalized to an arbitrary starting value of 1. Fluorescence recovery, or the loss of bleached fluorescence, was initially analyzed by assuming a single rate constant as described previously (Maddox *et al*., 2000). The dissociation rates were calculated as described previously (Maddox *et al*., 2000).

RESULTS

Gpa1 Interacts with Kar3

In a functional proteomics screen for proteins that interact with Gpa1, we identified the Fus3 MAPK (Metodiev *et al*., 2002) and the Kar3 microtubule-associated motor protein (Figure 1A and Supplemental Figure S1). Glutathione transferase (GST)-tagged Gpa1 was affinity purified from the lysates of vegetative and pheromone-treated cells. Proteins that copurified with Gpa1 were then visualized on two-dimensional gels, and those whose interaction with Gpa1 seemed to be stimulated by pheromone were identified by mass spectrometric analysis.

The putative association of Gpa1 and Kar3 was confirmed and further characterized in a series of reciprocal pull-down assays. In lysates of cells expressing tagged forms of both proteins from their native promoters, Kar3-HA copurified with GST-Gpa1 (Figure 1B, left). Conversely, the endogenous myristylated form of Gpa1 (bottom band) was readily detected in immunoprecipitates of Kar3-HA expressed from its own promoter (Figure 1B, right). As in the proteomic screen, pheromone treatment dramatically increased the amount of Kar3-HA that was pulled down with GST-Gpa1, as well as the amount of Gpa1 that coimmunoprecipitated with Kar3-HA. Because all G proteins change their affinity for their target proteins upon activation, the apparent enhancement of the Gpa1–Kar3 interaction could be due to the shift from Gpa1-GDP to Gpa1-GTP in pheromone-treated cells. Alternatively, the relatively higher efficacy of Gpa1/Kar3 pull-down from the lysates of pheromone-treated cells could be due to a higher level of Kar3, as pheromone induces the transcription of *KAR3* by 20-fold (Meluh and Rose, 1990). To test the latter possibility, we expressed KAR3-GST from the *CUP1* promoter, which is not regulated by phero-

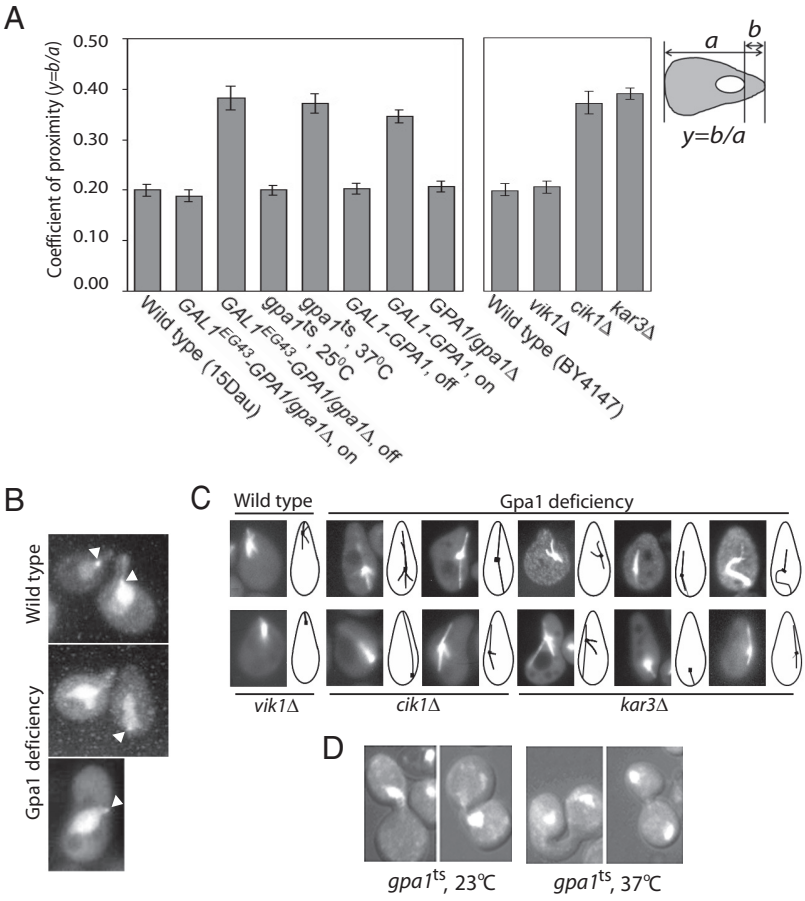

Figure 2. Effects of Gpa1 manipulation on microtubule organization and Kar3-dependent mating processes. (A) Aberrant Gpa1 expression and function confer a *kar3*Δ-like defect in pheromone-induced nuclear migration. Mid-log cells were treated with pheromone for 3 h. Their nuclei were then stained with DAPI and the mean of the ratio, b/a (distance from the nucleus to the shmoo tip divided by the cell length), was determined for each strain and condition ($n \geq 56$). Error bars indicate the SEM. At least 90% of the cells were shmooing in each culture; only shmooing cells were scored for nuclear position. The p values for each strain compared with wild type (15Dau) are as follows: 0.54×10^{-9} ($GAL1^{EG43}$-GPA1 turned off/gpa1Δ), 0.16×10^{-10} (*gpa1*^{ts} at 37°C), 0.26×10^{-13} (GAL1-GPA1 turned-on), 0.16×10^{-17} (*cik1*Δ), and 0.17×10^{-18} (*kar3*Δ). (B) Representative images used to quantify nuclear position (graphed in A). The arrowheads mark the position of the SPB. (C) Gpa1 deficiency confers a microtubule phenotype similar to those seen in *kar3*Δ and *cik1*Δ cells. Mid-log cells expressing *GFP-TUB1* were treated with pheromone and fluorescence images of shmoos were acquired after 3 h. Long and mislocalized microtubules were often seen in the Gpa1-deficient cells, as is the case in *kar3*Δ and *cik1*Δ cells. The percentage of normal cells in which the nucleus seemed to be connected to the shmoo tip by a single microtubule bundle ± SEP ($n = 200$) were as follows: wild type, 93 ± 1.8; *vik1*Δ, 98 ± 1.0; Gpa1-deficient, 40 ± 3.5; *kar3*Δ, 34 ± 3.3; and *cik1*Δ, 35 ± 3.5. (D) Gpa1 deficiency confers a *kar3*Δ-like defect in karyogamy. Bilateral *gpa1*^{ts} matings were performed for 3 and 5 h at the permissive and restrictive temperatures, respectively. The mating mixtures were then stained with DAPI and the proportion of recently fused cells with two nuclei was determined. Inactivation of Gpa1 significantly increased the proportion of binuclear cells: 3 ± 1.3% at 25°C versus 36 ± 3.7% at 37°C ($p < 0.0001$, $n = 160$; ± indicates the SEP).

mone. As shown in Figure 1C, pheromone greatly enhanced the Gpa1–Kar3 interaction even though the level of Kar3 did not change. This suggests that it is the pheromone-activation of one or more signaling elements, and not the change in *KAR3* expression, that augments the amount of associated Gpa1 and Kar3 in stimulated cells.

Does the Gpa1–Kar3 interaction require microtubules? Kar3 is a microtubule binding protein. Because some mammalian Gα proteins also bind microtubules, we wondered whether Gpa1 and Kar3 might copurify by virtue of a common affinity for microtubules. To test this possibility, we repeated the reciprocal pull-down assays in lysates made from cells treated first with nocodazole such that they reached full mitotic arrest, and then with pheromone. The Gpa1/Kar3 copurification yields were as robust in the nocodazole/pheromone-treated cells as in the control, despite the absence of polymerized tubulin (Figure 1D). This suggests that the Gpa1–Kar3 interaction is independent of microtubules.

Together, the results shown in Figure 1 indicate that Gpa1 and Kar3 interact in vivo, that this interaction is stimulated by pheromone, and that it is independent of both the level of Kar3 and the presence of polymerized tubulin.

Gpa1 Deficiency Mimics the Effects of kar3Δ and cik1Δ on Nuclear Migration, Cytoplasmic Microtubules, and Karyogamy

The absence of Kar3 in cells responding to pheromone confers significant defects in microtubule dynamics and nuclear migration (Maddox *et al*., 2003). Moreover, Kar3 is essential for nuclear congression after mating cells have fused (Meluh and Rose, 1990; Molk *et al*., 2006). If Gpa1 is an important regulator or mediator of Kar3 function, Gpa1 deficiency should mimic the defects conferred by *kar3*Δ. To test this, we used strains in which Gpa1 expression can be repressed (*GAL1-GPA1*), or in which Gpa1 can be inactivated (*gpa1*^{ts}). It is not possible to study *gpa1* null cells because *GPA1* is an essential gene.

Strain SLY168 conditionally expresses *GPA1* from the attenuated $GAL1^{EG43}$ promoter, which is ~1% as active as the native *GAL1* promoter (Giniger and Ptashne, 1988). When this strain was grown in galactose medium, the cells accumulated approximately twofold more Gpa1 than normal; 4 h after the $GAL1^{EG43}$-*GPA1* cells were shifted to glucose medium, their level of Gpa1 was ~50% of normal. We examined nuclear movement into the mating projections of pheromone-treated wild type, *kar3*Δ, *cik1*Δ, *vik1*Δ, and *gpa1*^{ts}, as well as of wild-type cells expressing Gpa1 from the full-strength *GAL1* promoter, and of $GAL1^{EG43}$-*GPA1* cells before and 4 h after Gpa1 expression had been turned off (Figure 2A). Both Cik1 and Vik1 are kinesin light chains that form heterodimers with Kar3, but only Cik1 is essential for the Kar3 mating functions (Page *et al*., 1994; Manning *et al*., 1999). After 2 h of pheromone treatment, the nucleus was always found near the shmoo tip in the wild-type and *vik1*Δ cells and in the *gpa1*^{ts} cells grown at permissive temperature. By comparison, the nuclei were found farther from the shmoo tip in the *kar3*Δ, *cik1*Δ, Gpa1 turn-off cells, high-level Gpa1-overexpressing cells, and *gpa1*^{ts} cells grown at restrictive temperature (p values all $<10^{-9}$). Furthermore, the

Table 3. Effect of Gpa1 deficiency, Gpa1 overexpression, and Gpa1 inactivation on microtubule orientation and dynamics

	Mean length captured Mts (μm)	Distally oriented Mts (%)	Shrinkage rate (μm s^{-1})	Shrinkage frequency (min^{-1})	Shrinkage duration (s)
Wild type, 30°C	1.33 ± 0.16 (n = 20)	23 ± 8 (n = 135)	0.05 ± 0.01 (n = 42)	0.42 ± 0.02 (n = 10)	34 ± 3 (n = 42)
$Gal1^{EG43}$-Gpa1 (off)[a]	2.27 ± 0.28* (n = 9)	31 ± 4++ (n = 100)	0.03 ± 0.004 (n = 6)	0.06 ± 0.003+ (n = 10)	32 ± 8 (n = 6)
Wild type, 23°C	1.42 ± 0.13 (n = 11)	29 ± 10 (n = 62)	0.02 ± 0.004 (n = 10)	0.42 ± 0.04 (n = 10)	66 ± 8 (n = 10)
Wild type, 37°C	1.45 ± 0.25 (n = 10)	21 ± 9 (n = 63)	0.04 ± 0.004 (n = 10)	0.68 ± 0.04 (n = 10)	35 ± 5 (n = 10)
$gpa1^{ts}$, 23°C	1.49 ± 0.20** (n = 10)	35 ± 11** (n = 60)	0.02 ± 0.002 (n = 9)	0.34 ± 0.06 (n = 10)	52 ± 6 (n = 9)
$gpa1^{ts}$, 37°C	2.50 ± 0.23*** (n = 10)	66 ± 11*** (n = 53)	0.05 ± 0.01 (n = 10)	0.22 ± 0.07** (n = 10)	33 ± 6 (n = 10)
$Gal1^{EG43}$-Gpa1 (on)[b]	ND	60 ± 11* (n = 80)	ND	ND	ND
$Gal1^{EG43}$-Gpa1 (on)[b], kar3Δ	ND	21 ± 3 (n = 78)	ND	ND	ND

Microtubule lengths, shrinkage rates, and shrinkage durations are reported as the mean ± SEM The percentages of distally oriented microtubules (Mts) and the shrinkage frequencies are reported as the mean ± SEP. *$p \leq 0.005$, **$p < 0.0005$, ***$p < 10^{-6}$, $^{+}p < 10^{-8}$, $^{++}p < 10^{-10}$. The statistical comparisons are as follows: *gpa1ts* cells at 37°C vs. wild-type cells at 37°C; *gpa1ts* cells at 23°C vs. *gpa1ts* cells at 37°C; all others vs. wild type at 30°C. ND, not determined.

[a] Glucose medium.

[b] Galactose medium.

nucleus seemed to be connected to the shmoo tip by a single microtubule bundle in >90% of the wild-type and *vik1*Δ cells, whereas less than half the *kar3*Δ, *cik1*Δ, and Gpa1 turn-off cells seemed normal in this regard (Figure 2C). The K21E R22E allele of *GPA1* was reported previously to confer a similar microtubule phenotype in this assay (Matheos *et al*., 2004). To determine whether Gpa1 plays a role in karyogamy, we scored for nuclear fusion in zygotes resulting from *gpa1ts* X *gpa1ts* matings at the permissive and restrictive temperatures. The results indicated that Gpa1 is required for normal karyogamy (Figure 2D). Together, the results of the cellular assays demonstrate that Gpa1, like Kar3 and Cik1, is required for pheromone-induced nuclear migration.

Gpa1 Affects Cytoplasmic Microtubule Orientation and Dynamics

The microtubule phenotypes shown in Figure 2B and in Matheos *et al*. (2004) could be due to abnormalities in microtubule orientation and/or dynamics. To distinguish these possibilities, we examined time-lapse movies of cytoplasmic microtubules in pheromone-treated wild-type, *gpa1ts*, and *GAL1EG43-GPA1* cells expressing *GFP-TUB1*. In all cases of aberrant Gpa1 expression and function, we observed a very significant loss of microtubule orientation (Table 3 and Supplemental Videos 1 and 2). Whereas most microtubules were oriented toward the shmoo tip in wild-type cells, the percentage of microtubules pointed away from the shmoo tip was significantly increased in the experimental strains. Deficient Gpa1 expression and inactivation of the temperature-sensitive form of Gpa1 also conferred some notable defects in microtubule dynamics. First, loss of Gpa1 increased the percentage of microtubule shrinkage events that were accompanied by a loss of cortical contact at the shmoo tip (Figure 3). The magnitude of this effect was similar to that reported for *kar3*Δ cells (Maddox *et al*., 2003). Second, the microtubules contacting any part of the cortex in Gpa1-deficient and *gpa1ts* cells were abnormally long, and this phenotype correlated with a decreased frequency of shrinkage events (Table 3). As shown in Figure 4 (and Supplemental Videos 1 and 2), the microtubules that contact the cortex in Gpa1-deficient cells tend to grow longer over time while spending relatively little time shrinking, compared with the dynamic instability exhibited by such microtubules in wild-type cells. Together, these data indicate that Gpa1 influences both the orientation and the dynamics of cytoplasmic microtubules in pheromone-treated cells.

Gpa1 Affects Cytoplasmic Microtubule Orientation Independently of Its Effects on Actin

In addition to its effect on the orientation of cytoplasmic microtubules, *gpa1K21E R22E* confers a modest defect in pheromone-induced actin polarization (Matheos *et al*., 2004). Because the plus ends of cytoplasmic microtubules are moved toward the mating projection along actin cables (Hwang *et al*., 2003), we considered the possibility that the microtubule

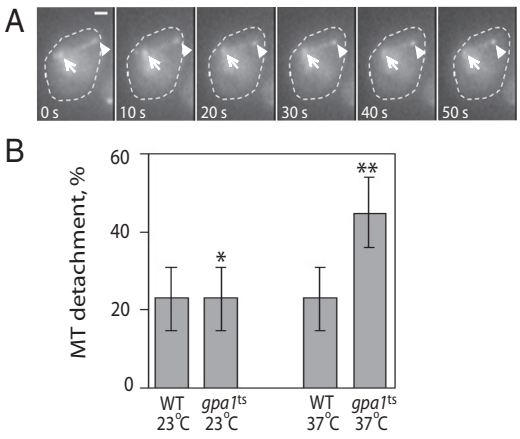

Figure 3. Loss of microtubule–cortex contact during catastrophe. (A) Example of a shmooing cell in which the microtubule bundle loses contact with the cortex upon shrinking. The arrows mark the position of the SPB; the arrowheads mark the plus end of the microtubule. The reporter was Kar3-GFP, which decorates the entire microtubule but has greatest affinity for the plus end and the SPB (Maddox *et al*., 2003). Bar, 1 μm. (B) Percentage of microtubule shrinkage events resulting in loss of cortical contact. Microtubule–cortex contact was considered to be lost if the SPB did not move toward the cortex during a shrinkage event. The bar graphs indicate the mean for a given strain and condition ± the SEP. In comparison to *gpa1ts* at 37°C (n = 50), **p = 0.0002 for wild-type cells at 37°C (n = 59), and *p = 0.0014 for *gpa1ts* cells at 23°C (n = 68). For wild-type cells at 23°C, n = 90.

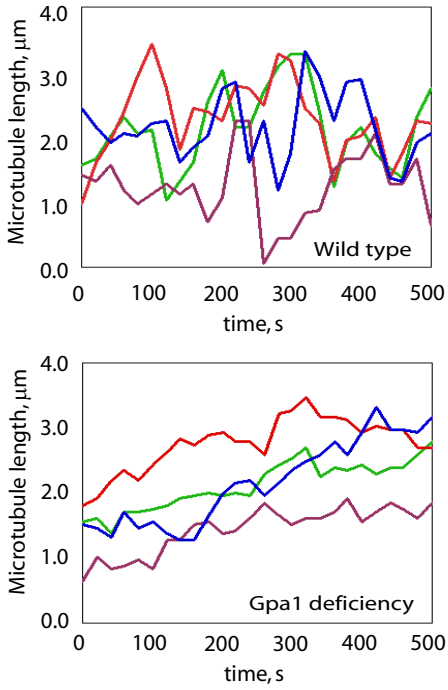

Figure 4. Dynamics of microtubules contacting the cortex in wild type and Gpa1-deficient cells. The lengths of microtubules that maintained contact with the cortex in shmooing cells were measured every 2 s for 500 s. Each of the line graphs represents the length changes in one randomly selected microtubule per cell over this interval. The microtubules in Gpa1-deficient shmoos are typically much less dynamic than those in the control cells.

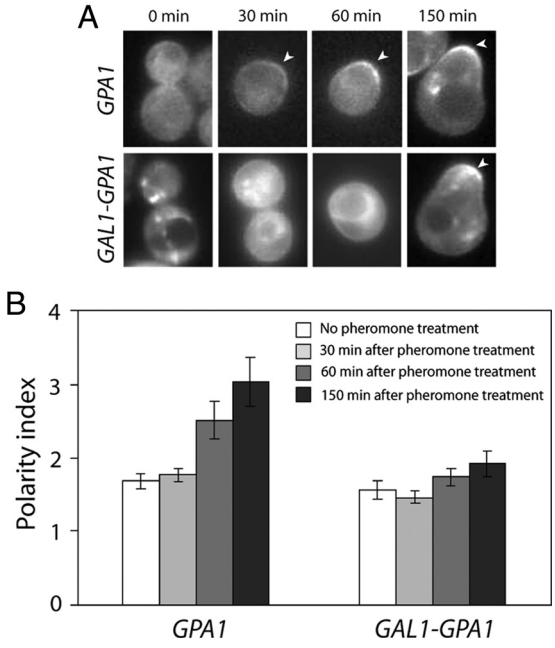

Figure 5. Pheromone-induced polarization of Gpa1. (A) Localization of Gpa1 in pheromone-treated cells. Mid-log cells expressing Gpa1-GFP from the *GPA1* promoter or overexpressing Gpa1-GFP from the *GAL1* promoter were treated with pheromone and fluorescence images were acquired at the indicated time points. Cells judged to be representative of the cultures at each time point are shown. Arrowheads mark the polarized membrane localization of the reporters. (B) Quantification of Gpa1 polarization. For cells that had not yet formed a mating projection, the degree of Gpa1-reporter polarization in a given cell (polarity index) was obtained by dividing the mean signal intensity in the brightest quarter of the plasma membrane by the mean signal intensity in the opposite quarter of the plasma membrane. For shmooing cells, the polarity index was obtained by dividing the mean signal intensity in the brightest seventh of the plasma membrane by the mean signal intensity in the opposite seventh of the plasma membrane. Bar graphs represent the mean of the polarity indices cells at each time point (n = 15); error bars indicate SEM. The wild type Gpa1-GFP reporter became significantly polarized before mating projection formation (for untreated vs. pheromone-treated Gpa1-GFP cells, $p = 0.0077$ at 60 min and $p = 0.0006$ at 150 min). In contrast, cells modestly overexpressing the Gpa1-GFP reporter from the *GAL1* promoter showed no significant polarization (comparing 0 min to 30, 60, and 150 min, the p values were 0.51, 0.33, and 0.10 for the Gal1-Gpa1-GFP cells, respectively).

orientation phenotypes resulting from changes in Gpa1 expression and function were due to loss of actin polarity. Alternatively, Gpa1 could affect microtubule orientation directly or via its interaction with Kar3. To determine whether the effect of Gpa1 expression on microtubule orientation could be due to the effect of Gpa1 on actin polarization, we asked whether the two polarity defects were correlated. Cells expressing *GFP-TUB1* were fixed 1–1.5 h after pheromone treatment, stained with rhodamine phalloidin, and scored for both actin and microtubule polarity (See Supplemental Figure S2 for representative images. The microtubule phenotypes conferred by changes in Gpa1 expression are also shown in Table 3). Gpa1 turn-off led to actin and microtubule polarity defects in ~67 and 70% of the cells, respectively, and the fraction of cells exhibiting both defects was slightly less than that predicted by chance alone (42 vs. 47%). Modest overexpression of Gpa1 conferred the same types of actin and microtubule polarity phenotypes, although in a smaller proportion of cells. Again, the coincidence of the actin and microtubule polarity defects was about what was expected to occur by chance (15 vs. 12%). Whether Gpa1 expression was aberrantly high or low, a large fraction of cells exhibited an obvious defect in microtubule polarity but no defect in actin polarity (65 and 39% for Gpa1-deficient and Gpa1-overepxressing cells, respectively). Although there is an unknown degree of error in characterizing the correspondence of actin and microtubule polarity defects by this method, these data taken at face value suggest that Gpa1 orients cytoplasmic microtubules in pheromone-treated cells by a mechanism independent of its effect on actin polarity, but do not preclude the possibility that Gpa1 also affects microtubule orientation indirectly via actin.

Gpa1 Positions and Stabilizes Microtubule–Cortex Interactions at Least Partly by a Kar3-dependent Mechanism

Several observation suggest that Gpa1 and Kar3 function together during mating: the interaction of Gpa1 with Kar3 (Figure 1), the impact of Gpa1 on the Kar3-dependent processes of nuclear movement and karyogamy (Figure 2), and the involvement of both Gpa1 (Figure 3) and Kar3 (Maddox *et al*., 2003) in the cortical attachment of shrinking microtubules. As shown in Figure 5, Gpa1 polarizes at the plasma membrane before morphogenesis, at about the same time that cytoplasmic microtubules are first captured at the future growth site (Maddox *et al*., 1999). Therefore, we wondered whether Gpa1 mediates the capture and/or cortical attach-

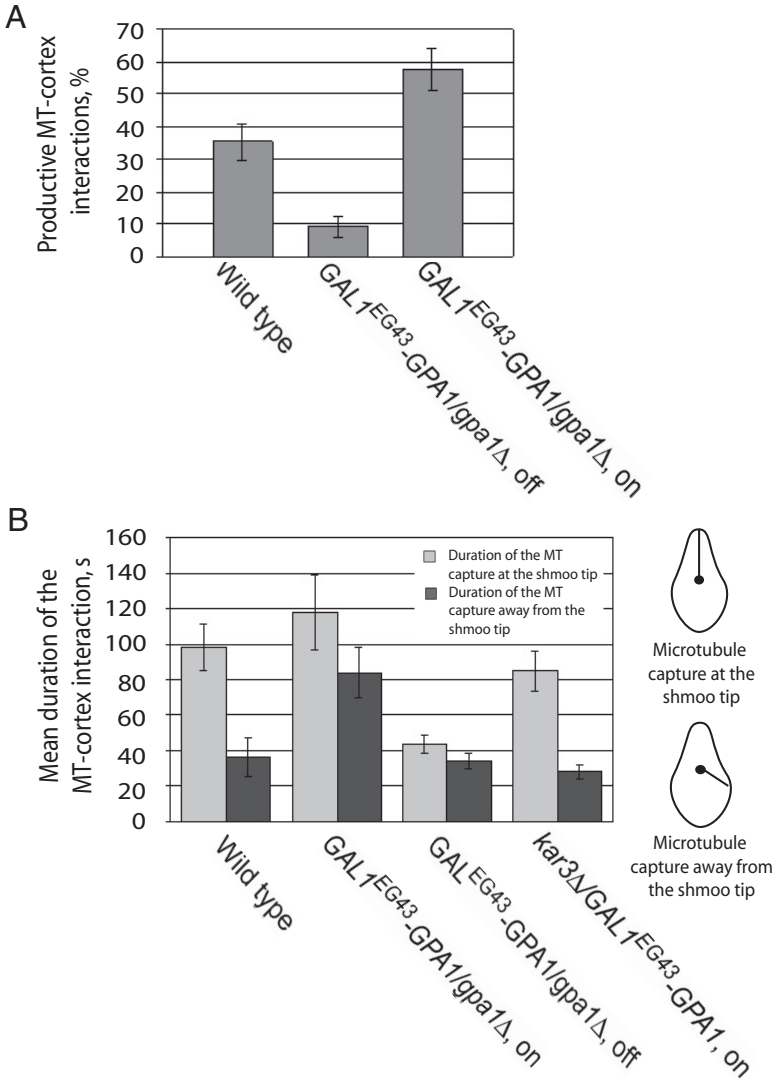

Figure 6. Effect of Gpa1 on microtubule–cortex interactions. (A) Gpa1 expression level positively correlates with the proportion of productive microtubule–cortex interactions. Pheromone-treated cells of the indicated genotypes and conditions were scored for the percentage of cortical contacts that resulted in movement of the SPB toward the shmoo tip by using *GFP-TUB1* as a reporter. The bar graphs indicate the mean for a given strain and condition ± the SEP. In comparison with the wild-type cells (n = 71), p = 0.004 for the Gpa1-overexpressing cells (n = 59) and p = 0.00002 for the Gpa1-deficient cells (n = 87). (B) Gpa1 influences the location and duration of microtubule–cortex interactions. Pheromone-treated cells of the indicated genotypes/conditions were analyzed to determine where their cytoplasmic microtubules were captured, and for how long. The bar graphs indicate the mean duration of contact for a given strain and condition ± SEM. Light bars indicate capture at the shmoo tip; dark bars indicate capture away from the shmoo tip. The significant differences are as follows: p = 0.002 for capture at (n = 20) versus away (n = 10) from the shmoo tip in wild-type cells; p = 0.008 for capture away from the shmoo tip in wild-type cells versus Gpa1-overexpressing cells (n = 12); p = 0.0002 for capture away from the shmoo tip in Gpa1-overexpressing versus Gpa1-overexpressing *kar3*Δ cells (n = 14); p = 0.0002 for capture at the shmoo tip in wild-type versus Gpa1-deficient cells (n = 20). The relevant insignificant differences are as follows: p = 0.21 for capture at the tip in wild-type versus Gpa1-overexpressing cells (n = 18); p = 0.06 for capture at (n = 20) versus away (n = 13) from the shmoo tip in Gpa1-deficient cells; p = 0.09 for capture at the tip in wild-type versus Gpa1-overexpressing *kar3*Δ cells (n = 18); p = 0.43 for capture away from the tip in wild type versus Gpa1-deficient cells (n = 13); p = 0.23 for capture away from the tip in wild-type versus Gpa1-overexpressing *kar3*Δ cells.

ment of microtubules via its interaction with Kar3. To test this hypothesis, we quantified the productive microtubule–cortex interactions in Gpa1-overexpressing, Gpa1-deficient, and control cells (Figure 6A). A productive interaction is defined as one in which microtubule contact anywhere on the cortex results in SPB movement. This requires a stable connection. In cells modestly overexpressing Gpa1, microtubule–cortex interactions were productive more often than in wild type cells (p = 0.004). Conversely, microtubule sampling of the cortex resulted in SPB movement much less often than normal in Gpa1-deficient cells ($p = 0.23 \times 10^{-4}$). These results suggest that Gpa1 plays a role in the attachment and/or shrinkage of microtubules at the cortex.

To differentiate between defects in capture and shrinkage, we quantified the effects of aberrant Gpa1 levels on the localization and duration of microtubule–cortex interactions (Figure 6B). In the control cells, microtubule-cortex interactions lasted ~3 times longer at the shmoo tip than away from it (p = 0.002), as expected from previous reports (Shaw *et al*., 1997; Maddox *et al*., 1999). In contrast, microtubule–cortex interactions were significantly shorter at the shmoo tips of Gpa1-deficient cells (p = 0.0002) and did not last significantly longer than elsewhere around these cells (p = 0.06). This suggests that the enhanced stability at the shmoo tip depends on Gpa1. Consistent with this, overexpression of Gpa1 increased the duration of microtubule–cortex interactions away from the shmoo tip (p = 0.008), without significantly affecting this measure at the shmoo tip (p = 0.21). The more uniform distribution of stable microtubule–cortex contacts around these cells correlates with the loss of Gpa1 polarity that results from Gpa1 overexpression (Figure 5). Notably, the effect of excess Gpa1 on microtubule–cortex interaction was completely suppressed by deletion of *KAR3* (Figure 6B). Just as in the control cells, microtubule-cortex interactions lasted ~3 times longer at the shmoo tip than away from it in cells overexpressing Gpa1 but lacking Kar3. The observation that *kar3*Δ is epistatic to Gpa1 overexpression in this assay is consistent with the idea that Kar3 is downstream of Gpa1 in the pathway connecting pheromone stimulation to microtubule-cortex interactions as suggested by the Gpa1–Kar3 interaction, although the data do not exclude the involvement of other factors or direct Gpa1–microtubule contact. Note that in the absence of Kar3, the bias of microtubule–cortex contact to the shmoo tip might be maintained by the interaction of microtubule plus ends with Kar9 or other factors. In contrast, Gpa1 deficiency confers a significant loss of microtubule-cortex contact at the shmoo tip. This suggests that Gpa1 interacts directly with microtu-

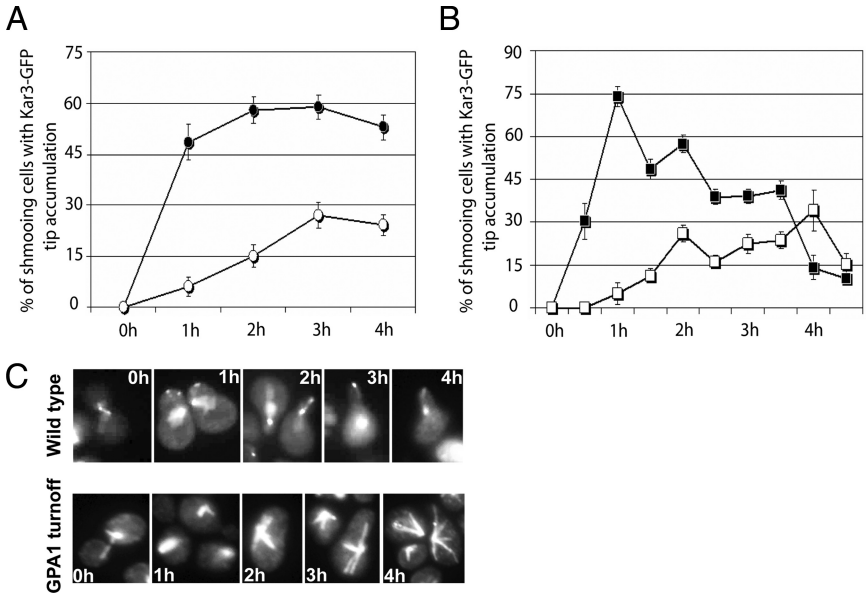

Figure 7. Accumulation of Kar3-GFP at the tips of shmooing cells is partially dependent on Gpa1. (A) Effect of Gpa1 inactivation on Kar3-GFP shmoo tip localization. *gpa1^{ts}* cells expressing Kar3-GFP were grown to mid-log phase at 23°C and either maintained at the permissive temperature or shifted to 37°C concomitant with pheromone treatment (0 time). Aliquots were taken and fluorescence images were acquired at the indicated time points. Data points represent the mean percentage of shmooing cells with clear fluorescence at their tips ± the SEP. Tips were examined in all focal planes. In comparison with *gpa1^{ts}* cells maintained at 23°C (closed circles), those shifted to 37°C (open circles) showed significantly weaker tip localization at each time point: $p = 0.024$ at 1 h ($n = 70$), $p = 0.003$ at 2 h ($n = 111$), $p = 0.0005$ at 3 h ($n = 129$), and $p = 0.0008$ at 4 h ($n = 184$). (B) Effect of Gpa1 deficiency on Kar3-GFP shmoo tip localization. Fluorescent images of pheromone-treated wild-type and Gpa1-deficient cells were acquired at the indicated time points and scored as described above. Data points represent the mean percentage of shmooing cells with clear fluorescence at their tips ± the SEP. In comparison with wild-type cells (closed squares), the Gpa1-deficient cells (open squares) showed significantly weaker Kar3-GFP tip localization until the control culture began to recover: $p = 0.0022$ at 1 h ($n = 10$), $p = 0.00013$ at 1.5 h ($n = 30$), $p = 0.016$ at 2 h ($n = 181$), $p = 0.030$ at 2.5 h ($n = 222$), $p = 0.036$ at 3 h ($n = 250$), and $p = 0.056$ at 3.5 h ($n = 200$). (C) Representative images used to quantify the effect of Gpa1 deficiency on Kar3-GFP localization (graphed in A).

bule plus ends or with other microtubule-associated proteins in addition to Kar3. Together, the data shown in Figure 6 indicate that Gpa1 is required for the maintenance of microtubule–cortex contact and that this function at least partially depends on Kar3 but do not allow us to determine whether Gpa1 also affects microtubule shrinkage.

Gpa1 Affects the Dynamic Association of Kar3 with Microtubule Plus Ends at the Shmoo Tip

Kar3 localizes to the plus ends of cytoplasmic microtubules and couples them to the cortex of the shmoo tip when they are shrinking (Maddox *et al*., 2003). Because Gpa1 interacts with Kar3 and is also highly concentrated at the shmoo tip, we wondered whether the cortical localization of Kar3 depends on Gpa1. To test this, we first asked whether Gpa1 inactivation or deficiency would affect the shmoo tip localization of a Kar3-GFP reporter. As shown in Figure 7, Kar3-GFP was slow to accumulate at the shmoo tip in cells either lacking (*gpa1^{ts}* cells at 37°C) or deficient (*GAL1^{EG43}-GPA1* cells in glucose) in Gpa1 function, and the peak percentage of experimental cells that showed a clear shmoo-tip signal was about half that observed in the relevant control cultures ($p < 0.05$ for both experiments). As a second test of the idea that Gpa1 regulates Kar3 localization, we evaluated the effect of aberrant Gpa1 expression and function on the turnover rates of the Kar3-GFP reporter at shmoo tips by using FRAP analysis (Reits and Neefjes, 2001). After the wild-type and experimental strains were treated with pheromone and allowed to form mating projections, the Kar3-GFP signal at the plus ends of shmoo-tip microtubules was photobleached, and the recovery of fluorescence was quantified and plotted against the time after photobleaching. As shown in Table 4, overexpression of Gpa1 from the full-strength *GAL1* promoter greatly increased the half-time for recovery.

Table 4. FRAP analysis of Kar3-GFP at microtubule plus ends near the shmoo tip

	k (rate of dissociation), a.u	$t_{1/2}$, s	R, % recovery
Wild type, glucose	0.104 ± 0.026	6.99 ± 1.61	58 ± 18
Wild type, galactose	0.115 ± 0.037	6.66 ± 3.03	62 ± 17
GAL1-GPA1 (on)[a]	0.050 ± 0.015^{+}	14.86 ± 3.76^{++}	63 ± 14
GAL1-GPA1 (off)[b]	0.094 ± 0.027	8.03 ± 2.24	60 ± 20
GAL1^{EG43}-GPA1/gpa1Δ (off)[b]	0.156 ± 0.047*	4.76 ± 1.17*	63 ± 16
GAL1^{EG43}-GPA1/gpa1Δ (on)[a]	0.097 ± 0.024	7.29 ± 1.52	56 ± 19
gpa1^{ts}, 37°C	0.222 ± 0.078**	3.35 ± 2.64^{+}	49 ± 23
gpa1^{ts}, 25°C	0.113 ± 0.067	6.79 ± 2.47	62 ± 16

All values are reported as the mean ± SD, $n = 10$ for each measurement. *$p \leq 0.01$, **$p \leq 10^{-3}$, $^{+}p \leq 10^{-4}$, $^{++}p < 10^{-5}$; The statistical comparisons are as follows: Cells overexpressing Gpa1 (lines 3 and 5) and cells deficient in Gpa1 (lines 4 and 6) vs. wild-type cells cultured in the corresponding medium (glucose or galactose), and *gpa1^{ts}* cells at 23°C vs. *gpa1^{ts}* cells at 37°C (lines 7 and 8).

[a] Galactose medium.

[b] Glucose medium.

Conversely, Gpa1 deficiency and inactivation of Gpa1 by shifting *gpa1^{ts}* cells to the restrictive temperature greatly decreased this measure. As a negative control, we photobleached the Kar3-GFP signal at the SPB of pheromone-treated cells. Here, the half-time for recovery was unaffected by manipulation of Gpa1. Together, the Kar3-GFP localization and FRAP data indicate that Gpa1 positively affects the association of Kar3 with microtubule plus ends in the mating projection, consistent with the idea that Gpa1 recruits Kar3-bound microtubules to the cortex at the shmoo tip.

DISCUSSION

The yeast mating reaction is a directional response. A mating yeast cell orients toward the strongest source of pheromone and grows in that direction. At the same time, the nucleus moves toward the tip of the mating projection. As the pheromone-induced polarization of growth and nuclear position depend on dynamic changes in F-actin and microtubule cables, these phenomena provide an opportunity to study regulation of the actin and microtubule cytoskeletons by an external signal.

In cells, cytoplasmic microtubules grow and shrink at their plus ends (Maddox *et al*., 1999), and Kar3 is required to maintain their cortical attachment as they shrink (Maddox *et al*., 2003). Recently, it has been shown that Cik1 targets Kar3 to microtubule plus ends and that the Kar3/Cik1 heterodimer triggers plus-end depolymerization in vitro (Sproul *et al*., 2005). On the basis of these results, it has been proposed that Kar3/Cik1 stimulates the plus-end depolymerization of cytoplasmic microtubules in mating cells while maintaining their cortical attachment, thus drawing the nucleus toward the shmoo tip (Maddox *et al*., 2003; Maddox, 2005; Molk and Bloom, 2006). This model raises two key questions: 1) What anchors Kar3 to the cortex? And 2) What, if anything, regulates Kar3-mediated depolymerization of the microtubules coupled to the cortex?

In an alternate but not mutually exclusive model of nuclear migration (Molk and Bloom, 2006), microtubules periodically lose contact with the shmoo tip and shrink back to the SPB. These are replaced by newly nucleated microtubules that are transported into the mating projection along actin cables. The nucleus is thus moved toward the shmoo tip as shorter and shorter microtubules bind to the cortex. Because Kar3 localizes to free as well as cortical microtubule plus ends (Maddox *et al*., 2003), cortical capture of Kar3-bound microtubules could contribute to this mechanism. It is also possible that individual microtubules in the attached bundle briefly lose contact with the cortex as they shorten and have to be recaptured (Maddox *et al*., 1999). Both of these scenarios require an element that captures Kar3-bound microtubule plus ends at the shmoo tip. Until now, there have been no candidates for this role.

In this investigation, we have shown that pheromone stimulates an interaction between Gpa1and Kar3 that does not depend on microtubules or increased transcription of either *GPA1* or *KAR3* (Figure 1), that Gpa1 positively affects the association of Kar3 with the plus ends of microtubules at the shmoo tip (Figure 7 and Table 4), and that Gpa1 stimulates productive microtubule–cortex interactions (Figure 6A). We have also shown that Gpa1 affects the position and duration of microtubule-cortex contact (Figure 6B) and that this effect depends on Kar3. Finally, we found that Gpa1 turn-off and temperature-sensitive inactivation caused detachment of the microtubules from the cortex during shrinkage events (Figure 3), as is seen in *kar3*Δ cells (Maddox *et al*., 2003). From these observations, we infer that Gpa1 is a cortical anchor for Kar3. As such, Gpa1 fills two postulated functions: It recruits Kar3-bound microtubule plus ends to the shmoo tip, and it helps to maintain microtubule–cortex contact during shrinkage events. In proposing that Gpa1 serves these functions, however, we do not imply that Gpa1 is the only Kar3 anchor. In fact, the partial Kar3-GFP mislocalization phenotype that results when Gpa1 is compromised suggests that there is at least one more such element. It is also possible that other proteins which interact with Gpa1 at the plasma membrane contribute to the observed regulation of microtubules in pheromone-treated cells. These include the Gpa1 GAP protein Sst2, the pheromone-specific Gβγ dimer, and the Fus3 MAP kinase. Although our results do not argue against the involvement of these elements, our data strongly suggest that Gpa1, a protein that polarizes on the membrane early in the pheromone response, helps to position and anchor microtubules at the growth site of mating cells by interacting with Kar3, a known microtubule binding protein.

Given that microtubule plus ends are localized to the mating projection along actin cables (Hwang *et al*., 2003), could the effect of Gpa1 perturbation on microtubules be entirely due to the impact of Gpa1on actin polarity? Our results argue strongly against this possibility. First, actin is not known to influence the stability and duration of microtubule-cortex contact, as do Kar3 and Gpa1 (Figures 3 and 6). Second, Gpa1 manipulation conferred obvious microtubule abnormalities in a large fraction of cells that displayed apparently normal actin polarity (Supplemental Figure S2). Third, there was no detectable pheromone-induced nuclear migration whatsoever in Gpa1-deficient cells, as in *kar3*Δ and *cik1*Δ cells (Figure 2). The severity of this phenotype is not consistent with the mild actin polarity defect conferred by Gpa1 deficiency. The simplest explanation of these data is that Gpa1 regulates microtubule orientation (i.e., localization to the mating projection) indirectly via actin, whereas Gpa1 affects microtubule-cortex contact and positioning via Kar3. Of course, the Gpa1–Kar3 interaction might also affect microtubule orientation.

Although the effects of Gpa1 on microtubule–cortex contact are readily explained as the direct consequences of Gpa1 binding to Kar3 and Kar3 binding to the plus ends of microtubules, Gpa1 may be more than merely a passive anchor for Kar3. The Gα protein seems to affect microtubule dynamics as well. Gpa1 deficiency and inactivation confer an increase in the mean length of microtubules contacting the cortex that correlates with a reduction in the number of shrinkage events (Table 3). It has been proposed that catastrophe is induced when microtubules contact the cortex of vegetative cells (Carminati and Stearns, 1997), and Sproul *et al*. (2005) have raised the possibility that plus-end depolymerization is stimulated at the cortex of the shmoo tip (Sproul *et al*., 2005). Given the infrequency of cortical microtubule shrinkage in Gpa1 turn-off and *gpa1^{ts}* cells, the regulator of microtubule catastrophe at the shmoo tip could be Gpa1. Through its interaction with Kar3, Gpa1 might bias the dynamic instability of microtubules attached at the shmoo tip so that shrinkage predominates over growth. It is also possible, of course, that Gpa1 affects microtubules directly. Mammalian Gα proteins have been reported to interact directly with tubulin (Wang *et al*., 1990; Chen *et al*., 2003). Our data do not distinguish between these possibilities.

In summary, the results presented here suggest that Gpa1 serves as an externally regulated positional determinant and anchor for Kar3, a previously unappreciated role for Gα proteins. We propose that by concentrating at the incipient mating projection, Gpa1 recruits Kar3-bound microtubule

plus ends to the shmoo tip and stabilizes their interaction with the cortex during shrinkage. Our data also suggest that Gpa1 positively regulates the frequency of microtubule shrinkage events at the cortex. By regulating both the localization of Kar3 and the initiation of microtubule shrinkage, Gpa1 may simultaneously ensure that the nuclear tether is appropriately positioned and that it shortens upon contacting the cortex.

ACKNOWLEDGMENTS

We thank Kerry Bloom and Jeff Molk for assisting in the FRAP analysis, Kerry Bloom and Vladimir Gelfand for helpful discussions, Dmitry Suchkov for automating the calculation of polarity indices, and Mark Longtine for critical reading of the manuscript. This work was supported by National Science Foundation grant MCB-0453964 to D.E.S. and National Institutes of Health grant GM-47337 (to J. C.).

REFERENCES

Acuto, O., and Cantrell, D. (2000). T cell activation and the cytoskeleton. Annu. Rev. Immunol. *18*, 165–184.

Affolter, M., and Weijer, C. J. (2005). Signaling to cytoskeletal dynamics during chemotaxis. Dev. Cell *9*, 19–34.

Ausubel, F. M., Brent, R., Kingston, R. E., Moore, D. D., Seidman, J. G., Smith, J. A., and Struhl, K. (1994). Current Protocols in Molecular Biology, New York, NY: John Wiley & Sons.

Ayscough, K. R., and Drubin, D. G. (1998). A role for the yeast actin cytoskeleton in pheromone receptor clustering and signalling. Curr. Biol. *8*, 927–930.

Bardwell, L. (2005). A walk-through of the yeast mating pheromone response pathway. Peptides *26*, 339–350.

Blackwell, E., Halatek, I. M., Kim, H. J., Ellicott, A. T., Obukhov, A. A., and Stone, D. E. (2003). Effect of the pheromone-responsive Gα and phosphatase proteins of *Saccharomyces cerevisiae* on the subcellular localization of the Fus3 mitogen-activated protein kinase. Mol. Cell Biol. *23*, 1135–1150.

Butty, A. C., Pryciak, P. M., Huang, L. S., Herskowitz, I., and Peter, M. (1998). The role of Far1p in linking the heterotrimeric G protein to polarity establishment proteins during yeast mating. Science *282*, 1511–1516.

Carminati, J. L., and Stearns, T. (1997). Microtubules orient the mitotic spindle in yeast through dynein-dependent interactions with the cell cortex. J. Cell Biol. *138*, 629–641.

Chen, N. F., Yu, J. Z., Skiba, N. P., Hamm, H. E., and Rasenick, M. M. (2003). A specific domain of Giα required for the transactivation of Giα by tubulin is implicated in the organization of cellular microtubules. J. Biol. Chem. *278*, 15285–15290.

Choi, K.-Y., Kranz, J. E., Mahanty, S. K., Park, K.-S., and Elion, E. A. (1999). Characterization of Fus3 localization: active Fus3 localizes in complexes of varying size and specific activity. Mol. Biol. Cell *10*, 1553–1568.

Gietz, R. D., and Sugino, A. (1988). New yeast—*Escherichia coli* shuttle vectors constructed with in vitro mutagenized yeast genes lacking six-base pair restriction sites. Gene *74*, 527–534.

Giniger, E., and Ptashne, M. (1988). Cooperative DNA binding of the yeast transcriptional activator GAL4. Proc. Natl. Acad. Sci. USA *85*, 382–386.

Goulimari, P., Knieling, H., Engel, U., and Grosse, R. (2008). LARG and mDia1 link Gα12/13 to cell polarity and microtubule dynamics. Mol. Biol. Cell *19*, 30–40.

Hwang, E., Kusch, J., Barral, Y., and Huffaker, T. C. (2003). Spindle orientation in *Saccharomyces cerevisiae* depends on the transport of microtubule ends along polarized actin cables. J. Cell Biol. *161*, 483–488.

Jackson, C. L., and Hartwell, L. H. (1990). Courtship in *S. cerevisiae*: both cell types choose mating partners by responding to the strongest pheromone signal. Cell *63*, 1039–1051.

Liu, J.-J., and Lindquist, S. (1999). Oligopeptide-repeat expansions modulate "protein only" inheritance in yeast. Nature *400*, 573–576.

Madden, K., and Snyder, M. (1998). Cell polarity and morphogenesis in budding yeast. Annu. Rev. Microbiol. *52*, 687–744.

Maddox, P., Chin, E., Mallavarapu, A., Yeh, E., Salmon, E. D., and Bloom, K. (1999). Microtubule dynamics from mating through the first zygotic division in the budding yeast *Saccharomyces cerevisiae*. J. Cell Biol. *144*, 977–987.

Maddox, P. S. (2005). Microtubules: Kar3 eats up the track. Curr. Biol. *15*, R622–R624.

Maddox, P. S., Bloom, K. S., and Salmon, E. D. (2000). The polarity and dynamics of microtubule assembly in the budding yeast *Saccharomyces cerevisiae*. Nat. Cell Biol. *2*, 36–41.

Maddox, P. S., Stemple, J. K., Satterwhite, L., Salmon, E. D., and Bloom, K. (2003). The minus end-directed motor Kar3 is required for coupling dynamic microtubule plus ends to the cortical shmoo tip in budding yeast. Curr. Biol. *13*, 1423–1428.

Manning, B. D., Barrett, J. G., Wallace, J. A., Granok, H., and Snyder, M. (1999). Differential regulation of the Kar3p kinesin-related protein by two associated proteins, Cik1p and Vik1p. J. Cell Biol. *144*, 1219–1233.

Martzen, M. R., McCraith, S. M., Spinelli, S. L., Torres, F. M., Fields, S., Grayhack, E. J., and Phizicky, E. M. (1999). A biochemical genomics approach for identifying genes by the activity of their products. Science *286*, 1153–1155.

Matheos, D., Metodiev, M., Muller, E., Stone, D., and Rose, M. D. (2004). Pheromone-induced polarization is dependent on the Fus3p MAPK acting through the formin Bni1p. J. Cell Biol. *165*, 99–109.

Meluh, P. B., and Rose, M. D. (1990). KAR3, a kinesin-related gene required for yeast nuclear fusion. Cell *60*, 1029–1041.

Metodiev, M. V., Matheos, D., Rose, M. D., and Stone, D. E. (2002). Regulation of MAPK function by direct interaction with the mating-specific Gα in yeast. Science *296*, 1483–1486.

Molk, J. N., and Bloom, K. (2006). Microtubule dynamics in the budding yeast mating pathway. J. Cell Sci. *119*, 3485–3490.

Molk, J. N., Salmon, E. D., and Bloom, K. (2006). Nuclear congression is driven by cytoplasmic microtubule plus end interactions in *S. cerevisiae*. J. Cell Biol. *172*, 27–39.

Musch, A. (2004). Microtubule organization and function in epithelial cells. Traffic *5*, 1–9.

Nern, A., and Arkowitz, R. A. (1999). A Cdc24p-Far1p-Gβγ protein complex required for yeast orientation during mating. J. Cell Biol. *144*, 1187–1202.

Page, B. D., Satterwhite, L. L., Rose, M. D., and Snyder, M. (1994). Localization of the Kar3 kinesin heavy chain-related protein requires the Cik1 interacting protein. J. Cell Biol. *124*, 507–519.

Pruyne, D., Legesse-Miller, A., Gao, L., Dong, Y., and Bretscher, A. (2004). Mechanisms of polarized growth and organelle segregation in yeast. Annu. Rev. Cell Dev. Biol. *20*, 559–591.

Reed, S. I., Hadwiger, J. A., and Lorincz, A. T. (1985). Protein kinase activity associated with the product of the yeast cell division cycle gene CDC28. Proc. Natl. Acad. Sci. USA *82*, 4055–4059.

Reits, E. A., and Neefjes, J. J. (2001). From fixed to FRAP: measuring protein mobility and activity in living cells. Nat. Cell Biol. *3*, E145–147.

Rose, M. D. (1996). Nuclear fusion in the yeast, *Saccharomyces cerevisiae*. Annu. Rev. Cell Dev. Biol. *12*, 663–695.

Shaw, S. L., Yeh, E., Maddox, P., Salmon, E. D., and Bloom, K. (1997). Astral microtubule dynamics in yeast: a microtubule-based searching mechanism for spindle orientation and nuclear migration into the bud. J. Cell Biol. *139*, 985–994.

Sherman, F., Fink, G. R., Hicks, J. B., Eds. (1986). Laboratory Course Manual for Methods in Yeast Genetics, Cold Spring Harbor, NY: Cold Spring Harbor Laboratory Press.

Sproul, L. R., Anderson, D. J., Mackey, A. T., Saunders, W. S., and Gilbert, S. P. (2005). Cik1 targets the minus-end kinesin depolymerase kar3 to microtubule plus ends. Curr. Biol. *15*, 1420–1427.

Stone, D. E., Cole, G. M., Lopes, M., Goebl, M., and Reed, S. I. (1991). N-myristoylation is required for function of the pheromone-responsive Gα protein of yeast: conditional activation of the pheromone response by a temperature-sensitive N-myristoyl transferase. Genes Dev. *5*, 1969–1981.

vanDrogen, F., Stucke, V. M., Jorritsma, G., and Peter, M. (2001). MAP kinase dynamics in response to pheromones in budding yeast. Nat. Cell Biol. *3*, 1051–1059.

Wach, A. (1996). PCR-synthesis of marker cassettes with long flanking homology regions for gene disruptions in *S. cerevisiae*. Yeast *12*, 259–265.

Wang, N., Yan, K., and Rasenick, M. M. (1990). Tubulin binds specifically to the signal-transducing proteins, Gsα and Giα 1. J. Biol. Chem. *265*, 1239–1242.

Winzeler, E. A., *et al*. (1999). Functional characterization of the *S. cerevisiae* genome by gene deletion and parallel analysis. Science *285*, 901–906.